Avances en la Investigación en Metalurgia y Materiales 2012

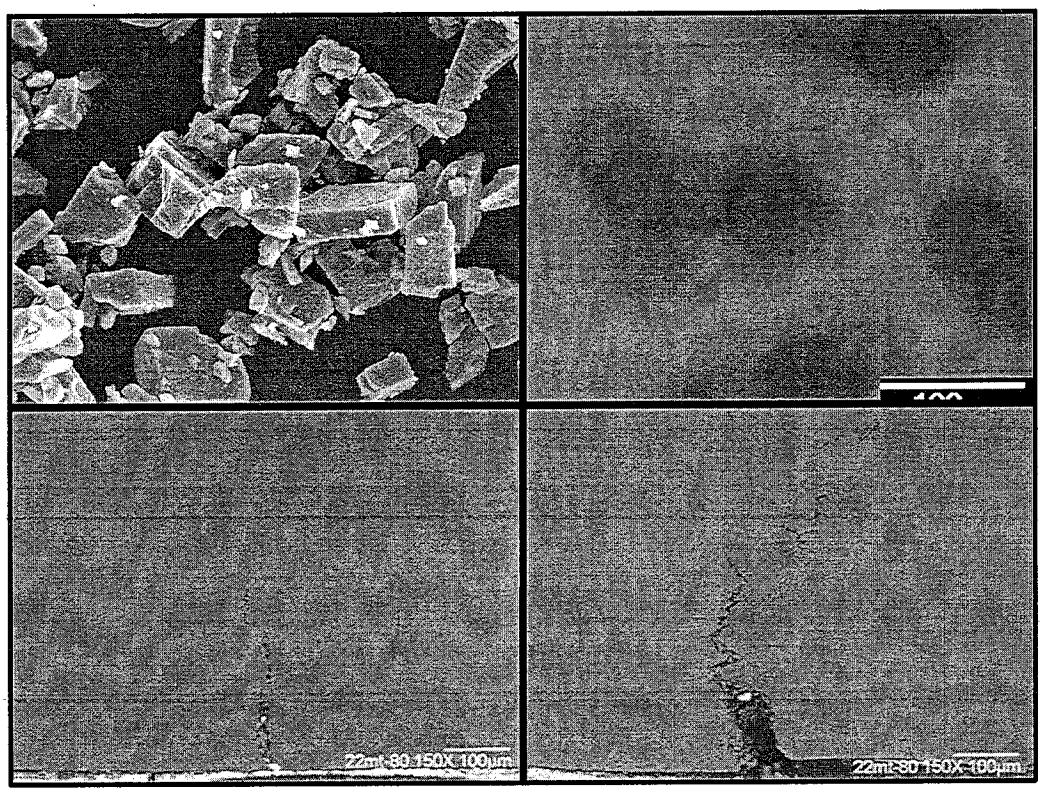

Editado
CA Tecnología de Soldadura y Unión de Materiales UMSNH-CA-209
CA Ciencia e Ingeniería de los Materiales UAdeC
ISBN 978-607-00-6215-5

Avances en la Investigación en Metalurgia y Materiales 2012

Comité Editorial: Víctor Hugo López Morelos, Ma. Gloria Rosales Sosa. Facultad de Metalurgia de la Universidad Autónoma de Coahuila e Instituto de Investigaciones Metalúrgicas de la Universidad Michoacana

Primera Edición Octubre 2012

ISBN: 978-607-00-6215-5

Impreso en México
Printed in Mexico

EDITORIAL VALLE DE CÁNDAMO
VERACRUZ 1403 INT. A, COL. LOS PINOS
MONCLOVA, COAHUILA, MEXICO
www.editorialvalledecandamo.com.mx
edit_valle_de_candamo@hotmail.com
TELS. 01 (866) 635-01-55 C.P. 25720

GROWTH OF ANATASE TiO_2 THIN FILMS INSIDE FUSED SILICA TUBING BY AACVD AND EVALUATION OF THEIR PHOTOCATALYTIC PROPERTIES

E. Ríos-Valdovinos, F. Pola-Albores, P. Amézaga-Madrid, P. Pizá-Ruiz, W. Antúnez-Flores, O. Solis-Canto and M. Miki-Yoshida*

*E-mail: mario.miki@cimav.edu.mx

Centro de Investigación en Materiales Avanzados and Laboratorio Nacional de Nanotecnología, Miguel de Cervantes 120, C. P. 31109, Chihuahua, Chih., México.

Introduction

Since Fujishima and Honda discovered the photocatalytic water splitting using electrodes of TiO_2 in 1972 [1], further researches have focused in the application of TiO_2 in different fields such as material science and environmental engineering applications [2-5]. In recent years, heterogeneous photocatalysis has increased their attention by the use of TiO_2 as photocatalyst; because its high photocatalytic activity, chemical stability and no toxicity properties [6]. TiO_2, in different forms such as powders and thin films, is attractive as photocatalyst in several reactions, in liquid or gas phase, by the generation of electron-hole pairs, and subsequent interaction with adsorbed species (OH^-, O_2) [7, 8].

TiO_2 used in the form of powder particles increases the photocatalytic efficiency due to the high surface area of the material, but it is necessary a final separation step to recover and to recycle it [9, 10]. In order to avoid this problem it is convenient to use the material immobilized as a thin film on inert substrate such as glass or ceramic, because in this way separation of the photocatalyst from the clean water is avoided, reducing processing time and cost, so leading to a wider range of applications [11, 12]. TiO_2 thin films can be prepared by numerous techniques such as spray pyrolysis [13], sol-gel [14], RF magnetron sputtering [15], pulsed laser deposition [16] and aerosol assisted CVD (AACVD) [17]. Among these techniques, AACVD provides more advantages because it has a relatively low cost; the microstructure, composition and thickness of the films can be controlled and the film could be obtained on flat substrates or inside and outside of tubing walls. In this work, Anatase TiO_2 thin films have been deposited inside of fused silica tubing by AACVD; its photocatalytic activity under external UV-Vis irradiation at room temperature was studied.

Experimental section

Synthesis of TiO_2 thin films

TiO_2 thin films were grown inside of fused silica tubing at several deposition temperatures from 300 to 500 °C, in steps of 50°C, by AACVD technique. The overall dimensions of the tubing were inside diameter (ID) of 13 mm and length (L) of 900 mm (Corning 7913). Details of the growth process by spraying an aerosol generated ultrasonically have been described elsewhere [18]. The diagram of the AACVD system is shown in Figure 1.

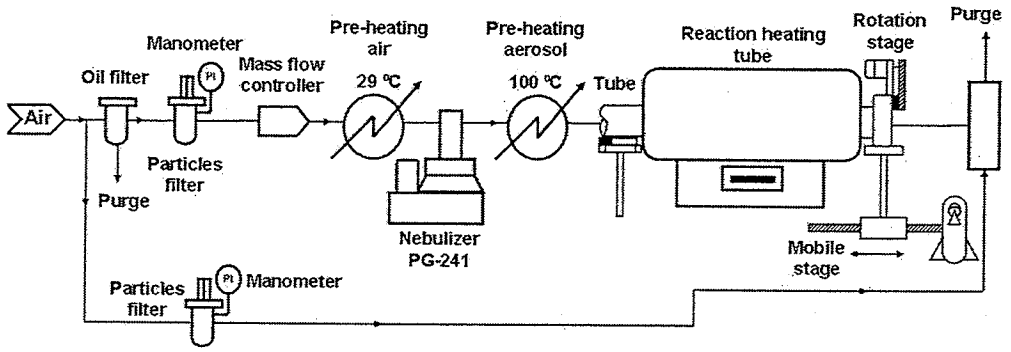

Figure 1. Schematic diagram of the system to growth TiO_2 thin films into fused silica tubing by AACVD.

Thin film characterization

The chemical precursor for the synthesis of TiO_2 thin films was characterized by X-Ray diffraction (XRD). This analyze was required to obtain the minimum temperature of TiO_2 growth and to optimize the substrate temperature at which the precursor was vaporized and was maintained during AACVD process. The XRD patterns were collected on XPert-Pro Panalytical diffractometer using Cu-Kα radiation (λ=1.54187 Å) at 40 kV and 30 mA. Approximately 0.5 g of sample was placed in the heating stage. Measurements were obtained from 25°C to 600°C in 2θ range of 10-65 degrees at the scanning rate of 2° min^{-1}.

Crystallographic properties of the TiO_2 thin films were investigated by using Grazing Incidence X-Ray Diffraction (GIXRD) configuration. The GIXRD patterns were collected on XPert-Pro Panalytical diffractometer using Cu-Kα radiation (λ=1.54187 Å) at 40 kV and 30 mA. The scanning rate was 1° min^{-1} at 0.05° step size from 25° to 60° in 2θ range. The incident beam angle was 0.5°. The identification of phases and the crystal structure of the

chemical precursor and the TiO_2 thin films were obtained by International Center for Diffraction Data (ICDD) with PDF cards. The crystallites size of TiO_2, **d**, was determined according the Scherrer's formula ($d=K\lambda/B \cos \theta$) [19]. We using the full width at half maximum (FWHM) data and considering the instrumental broadening previously determined (0.28°).

Raman spectroscopy was employed to complement the GIXRD results. The Spectra-Raman analyses of TiO_2 thin films were taken using a Micro Raman JoribaJobin Yvon LabRam HR spectrometer, equipped with a 632.8 nm Helium-Neon laser, from 50-800 cm^{-1} at room temperature and with a micro-Raman spot size of 10 microns.

Optical transmittance was determined using a Varian Cary 5000 UV-Vis- NIR spectrophotometer in the wavelength range of 300-1100 nm, with a scanning speed of 240 nm min^{-1}. Initially, the films were performed by depositing it on borosilicate glass substrates in order to analyze its optical properties. Uncoated glass substrate was used as a blank.

The surface morphology and the Root-Mean-Square (RMS) roughness of the films were analyzed by Atomic Force Microscopy (AFM) using a Digital Instruments Veeco Multimode Nanoscope IV-a system. AFM images were collected in Tapping Mode, with a sharpened tip at a scan rate of 1.0 Hz. Tapping Mode etched silicon probe (TESP) had a nominal tip radius of 5-10 nm, a cantilever length of 125 μm and a resonance frequency of 200-400 Hz. The average grain size and the average RMS roughness were calculated from images taken at 3X3 μm, 1X1 μm and 0.5X0.5 μm.

The morphology, composition and cross-section of the TiO_2 films were investigated by field emission scanning electron microscopy (FE-SEM) using a JEOL JSM-7401F operated at 2 kV and coupled to an X-Ray Energy Dispersive Spectrometer (EDS). SEM samples were cut into pieces (4 cm) and immobilized in the sample stage in order to allow cross section observations and then to calculate the average thickness of the samples.

Photocatalytic activity measurement

Photocatalytic activity of the films was evaluated by photo-decolorization of methylene blue (MB, $C_{16}H_{18}CIN3S.3H_2O$, Sigma) in aqueous solution under external UV-VIS irradiation at room temperature. The structure and the UV-Vis spectrum of the MB are shown in Fig. 2a and 2b, respectively. The UV-Vis spectrum of MB shows three absorption maxima at 241, 296

and 665 nm. The absorption band at 665 nm, which is the maximum peak, was used to quantify the photo-decolorization of MB solution. First, MB solutions of analytical grade were prepared at different concentrations from $1x10^{-3}$ to $1x10^{-10}$ mol dm^{-3} to find the relation between concentration and absorbance of MB solution. The absorbance spectrum of the MB solutions was measured using a UV-VIS Perkin Elmer Lambda 10 spectrophotometer, recorded from 220 to 800 nm and equipped with a fused silica cell having a path length of 1cm. A calibration curve (shown in Fig. 3) could be obtained with the maximum absorbance and with concentration of MB solutions. The tri-distillated water was used as reference.

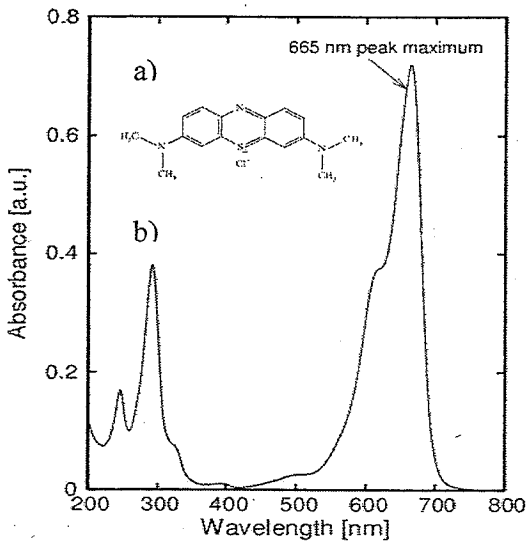

Fig. 2. a) MB structure (molar mass = 373.9 g mol^{-1}) and b) The UV-Vis spectrum of MB.

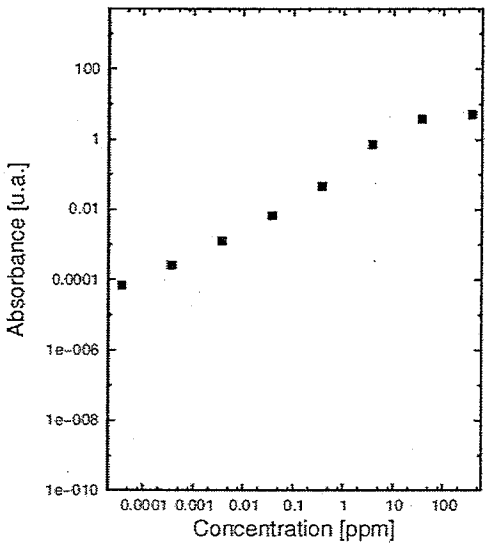

Fig. 3. Calibration curve of absorbance as a function of MB solution concentration.

Second, the photodecomposition measurements were carried out in TiO_2 film coated tubing with a section of 8 cm length, which was used as batch reactor. Fig. 4 shows the schematic representation of the exposition camera used for the photocatalytic evaluation. The radiation source was UV-Vis lamp (Blue Ray with maximum emission of 365 nm) and was put in at the camera center; its irradiance was measured using a PMA21100 UVA radiometer, this value was 8 mW cm^{-2}. Films coated tubings were filled with 10 cm^3 of MB solution and were placed around of the lamp at 1 cm of distance to obtain the desired irradiation. During the photocatalytic test, Nitrogen gas flow was inlet into the batch reactors and was kept at 0.05

L min^{-1}, to obtain movement constantly in the MB solution. The samples were exposed to irradiation of UV-Vis lamp at certain time intervals and the progress of the reaction was followed by monitoring the absorbance spectrum of MB solution at 665 nm every 20 min, in the range of 220 to 800 nm, using tri-distilled water as a blank. For comparison, the same procedure was also done for uncovered Vycor tubing.

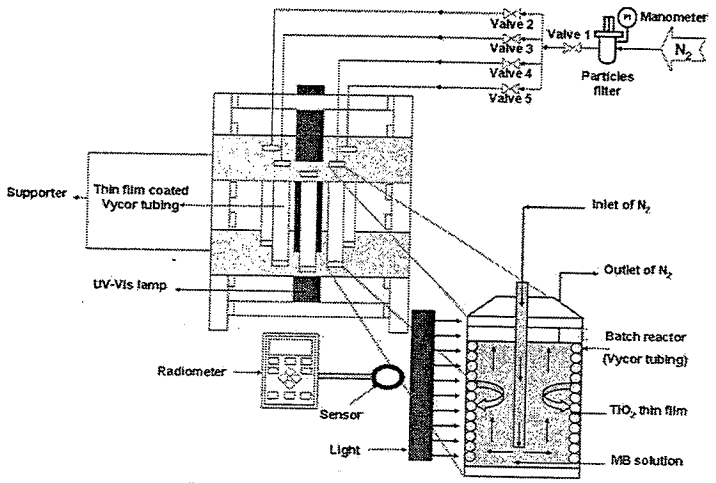

Figure 4. Schematic representation of the exposition camera used for the photocatalytic evaluation.

The activity was obtained as a function of irradiation time, several intervals between 20 to 100 minutes was tested; the MB concentration and irradiation intensity were kept at $1x10^{-5}$ mol dm^{-3} and 8 mW cm^{-2}, respectively. As well, to evaluate the effect of thickness on the activity, two samples were prepared at 1 and 2 steps; the MB concentration, irradiation time and irradiation intensity were kept at $1x10^{-5}$ mol dm^{-3}, 100 min and 8 mW cm^{-2} respectively.

The loss of activity was examined based on repeatedly the same sample under MB degradation and irradiation for four successive cycles; the MB concentration, irradiation time, irradiation intensity were kept at $1x10^{-5}$ mol dm^{-3}, 240 min and 8 mW cm^{-2}, respectively. For this examination the samples were previously cleaned with tri-distillated water and were dried at room temperature. Moreover, to study the influence of the regeneration on the photocatalytic activity, the samples were ultrasonic treated with tri-distillated water for 10 minutes and were dried at room temperature; the MB concentration, irradiation time, irradiation intensity were kept at $1x10^{-5}$ mol dm^{-3}, 240 min and 8 mW cm^{-2}, respectively.

Results and discussion

Thermal decomposition of chemical precursor by XRD

The XRD patterns of chemical precursor thermal decomposition from 25 °C to 600 °C are shown in Figure 5. The pattern at 25 °C only has the peaks corresponding to oxobis(acetylacetonate) $(C_5H_8O_2)_2TiO$ (JCPDS Card No. 35-1778) [20]. At 100 °C the precursor has not change in its structure and it has the same phase. When the temperature is increased at 200°C and 300 °C the precursor fully decomposes and is evident the amorphous phase. It has been reported that at 300 °C the crystallization of TiO_2 is affected because has much of carbon remained in its structure. Finally, TiO_2 is transformed to polycrystalline structure of anatase (JCPDS Card No. 21-1272) [20] with increasing the temperature from 400 to 600°C. Two Platinum reflexions (JCPDS Card No. 04-0802) [20] are evident in 2θ range at 39.80° and 46.28° in all patterns due to sample stage.

Structural and optical properties of TiO_2 thin films

Figure 6 shows the GIXRD patterns of TiO_2 thin films obtained inside Silica fused tubing by AACVD method at various substrate temperatures from 300 to 500 °C. TiO_2 film deposited at 300 °C does not exhibit any diffraction peak and the phase is amorphous. This result is in agreement with the previous reports stating the amorphous nature of the TiO_2 deposited at lower temperatures around 300 °C [21, 22]. When the temperature is increased at 350 °C the amorphous phase is crystallized and the anatase single phase of TiO_2 is formed with a tetragonal structure according to the PDF Card No 21-1272 [20]. At 400 °C the same phase is present and we can see an increment in the peak at (101) crystal plane. At 450 °C TiO_2 anatase exhibits seven peaks in the (101), (004), (112), (200), (105), (211) and (204) crystal planes, (101) being the predominant peak. When the temperature is 500 °C only the peak at (101) is shown. No significant impurities or a second phase were observed, which indicates that high-purity TiO_2 thin film is obtained.

These results are in agreement with XRD results that indicated the formation of TiO_2 by complete decomposition of the chemical precursor. The crystallite sizes of the TiO_2 thin films deposited at 450°C, were estimated from GIXRD results considering the (101) crystal plane using the Scherrer`s equation. The crystallite sizes at 1 and 2 steps were calculated as 54 and 41 nm, respectively.

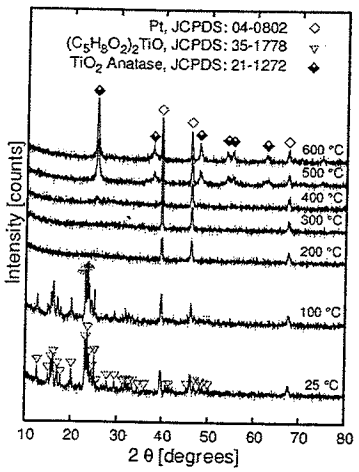

Fig. 5. XRD patterns of the thermal decomposition of $(C_5H_8O_2)_2TiO$ chemical precursor.

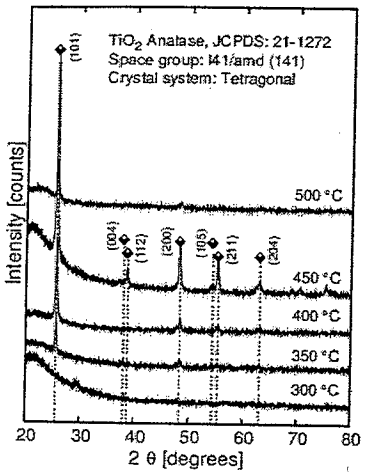

Fig. 6. GIXRD patterns of TiO_2 thin films grown by AACVD from 300 to 500°C.

Raman spectroscopy was used to investigate the presence of the crystal phases of the synthesized TiO_2 films. Figure 7 shows the Raman spectra of TiO_2 films obtained at 400, 450 and 500 °C. The Raman spectra for all the samples reveal well defined peaks at the following wavebands: 144 cm^{-1}, 197 cm^{-1}, 399 cm^{-1}, 513 cm^{-1} and 639 cm^{-1} ranging between 100 and 800 cm^{-1}. These wavebands have been assigned to three kinds of active Raman modes $A_{1g}+2B_{1g}+3E_g$ and are agreement with a previous spectrum of anatase TiO_2 crystal identified by Ohsaka [23]. The absence of peaks corresponding to another phase in the Raman spectra confirms the formation of purely anatase TiO_2. This finding is agreement with the results obtained by XRD and GIXRD measurements. In this work the lower temperature to TiO_2 thin films deposition was chosen at 450°C.

Figure 8 shows the UV-Vis transmittance spectra of TiO_2 films at 115 and 155 nm of thickness prepared at 450°C. Transmittance of the glass substrate is also shown as a reference. In both films can be seen the presence of interference fringes in the transmission spectrum from 400 to 1100 nm and a sharp absorption edge.

The two films are transparent to visible light and have above of 90% of transmittance in this region, but their transparency exhibits a sharp decrease in the UV range owing to the absorption of light. For substrate, the transmittance in visible region is of 92% and has too a sharp decrease in the UV range.

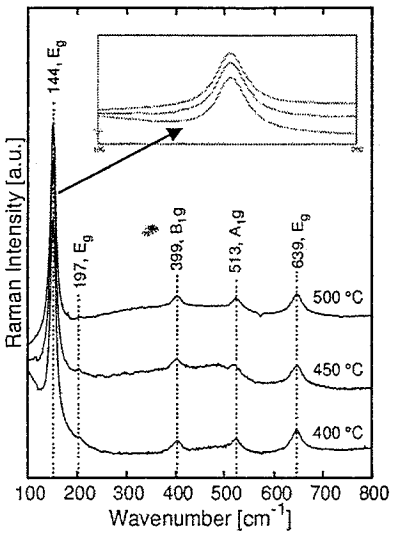

Fig. 7. Raman spectra of TiO_2 thin films growth at a) 400°C, b) 450°C and c) 500°C.

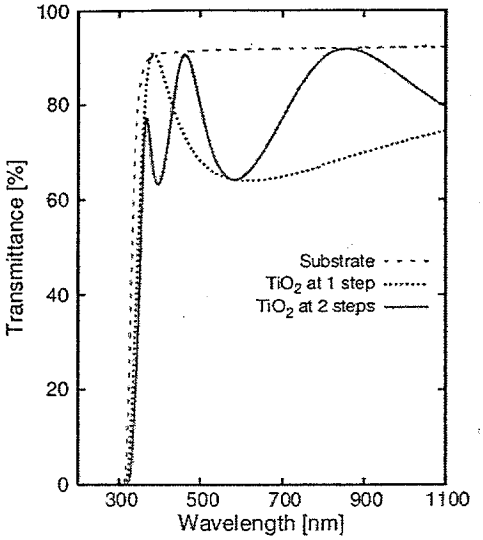

Fig. 8. Transmission spectrum of TiO_2 thin films deposited at 1 and 2 steps.

Tapping-mode atomic force microscopy images were taken in order to get information about the surface topography and the roughness of the films. The three-dimensional AFM image of TiO_2 thin film, obtained at 450°C, showed an initial spherical appearance and smooth surface. The average grain size for the samples prepared at 1 and 2 steps were estimated as 47 and 38 nm, respectively. These values are in accordance with the results obtained with the Scherrer's formula. Average RMS roughness analysis based on the AFM topography images were calculated as 4.25 and 3.19, respectively.

SEM secondary electron images of TiO_2 thin films obtained at 450 °C and deposited at 1 and 2 step shows that the samples produced were polycrystalline, homogeneous, uniforms and highly adherents to the substrate. Small grains with dense structure and well surface coverage are observed in both films. The film thicknesses were estimated by SEM analysis of the cross sectional of the TiO_2 films given in Fig 9a and 9b. They were calculated as 115 and 155 nm after 1 and 2 steps. Corresponding X-ray Energy Dispersive Spectroscopy (EDS) indicated the presence of elements as Ti and O. Additionally, Si, Na and Al were present in the samples, which were contained in the substrate.

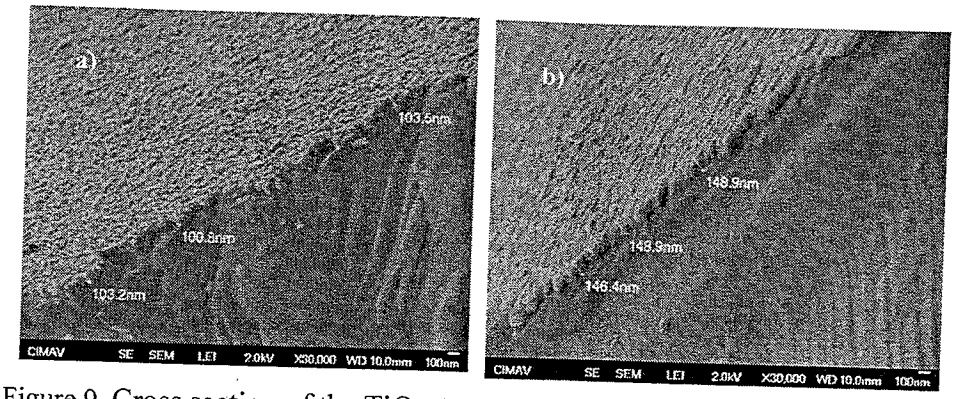

Figure 9. Cross section of the TiO_2 thin films deposited at a) 1 step and b) 2 steps.

Photo-decolorization of MB on TiO_2 thin films

The curve of calibration of absorbance, which was measured around 665 nm, as a function of MB solution concentration, **[C]**, is shown in Fig. 3. Further, linear fitting between absorbance and concentration of MB solution can be expressed as follows:

$$\mathbf{ABS = 0.1051 \bullet [C] + 0.00004} \qquad (1)$$

This calibration was used to quantify the final concentration of irradiated MB solutions.

According to numerous works [24-26], the photocatalytic decolorization of this dye is described by pseudo-first kinetic order. The photodecolorization kinetic constants of MB were calculated from the slope of the semilogarithmic plot colour (peak absorbance at λ_{max}=665 for MB) versus exposition time. According to Beer's law, the absorbance at 665 nm (the characteristic absorption wavelength of MB) is proportional to the concentration of MB in the reaction solution, so $\ln(C/C_0)$ equates to $\ln(A/A_0)$. The next equation was introduced as follow:

$$\mathbf{\ln(C_0 / C_t) = k_{app} * t = \ln(A_0 / A_t) = k_{app} * t} \qquad (2)$$

where $\mathbf{C_0}$ (g L^{-1}) is the initial concentration of MB solution at irradiation time 0, $\mathbf{C_t}$ (g L^{-1}) is the concentration of MB solution at reaction time **t** (min) after of UV-Vis irradiation and $\mathbf{k_{app}}$ is the apparent pseudo-first-order decolorization kinetic constant expressed in min^{-1}. A_0 is the solution absorbance at time zero and A is the solution absorbance at time t after turning on the lamp. For two TiO_2 thin films, prepared at 1 an 2 steps, the $\ln(A_0/A_t)$ was directly proportional to irradiation time. The slopes of apparent pseudo-first-order kinetics of

photocatalytic decolorization of MB solution, repeatedly the same sample at four successive cycles, as a function of irradiation time are presented in Table 1. The degradation rate of MB was calculated based on the following equation [25]:

$$\text{Degradation rate}(\%) = (C_0 - C_t)/C_0 \times 100 \quad (3)$$

where C_0 (g L^{-1}) is the initial concentration of MB solution at irradiation time 0 and C_t (g L^{-1}) is the concentration of the MB solution at reaction time t (min). In table 1, we can see the values of the degradation rates of MB solution for the repeated four cycles. It is evidently, that the degradation rate of MB decreases with increasing of cycles. As the samples are repeated use in the four cycles, there are more intermediate products being adsorbed on the TiO_2 thin films surface, which result in decrease of active sites.

Table 1. Values obtained of starting time, degradation rate, kinetic constant, initial rate constant and catalyst activity for successive cycles for TiO_2 films prepared at 1 (T10) and 2 (T11) steps.

Sample	No of cycle	t[a] (h)	D[b] (%)	Kapp[c] (min^{-1})	r_{0i}[d] (min^{-1} mol dm^{-3})	Catalyst activity
T10-0	1	0.0	60.07	0.0094	9.4321×10^{-8}	1
T10-1	2	1.6	58.46	0.0088	8.8300×10^{-8}	0.9361
T10-2	3	3.3	48.84	0.0079	7.9269×10^{-8}	0.8404
T10-3	4	5.0	47.3	0.0059	5.9201×10^{-8}	0.6276
T10-R	5	6.6	59.31	0.01	1.0034×10^{-7}	1
T11-0	1	0.0	39.19	0.0049	4.9167×10^{-8}	1
T11-1	2	1.6	32.52	0.0043	4.3146×10^{-8}	0.8775
T11-2	3	3.3	29.57	0.0036	3.6123×10^{8}	0.7346
T11-3	4	5.0	24.29	0.0033	3.3112×10^{-8}	0.6734
T11-R	5	6.6	29.2	0.0031	3.2194×10^{-8}	1

a Starting time of each cycle (cumulative) b Degradation rate of methylene blue
c Apparent pseudo-first-order decolorization kinetic constant
d Initial rate of photo-decolorization of methylene blue

Catalyst activity and loss activity

The initial rate of reaction, $\mathbf{r_{0i}}$, was obtained using the next equation:

$$-\mathbf{r_{0i}} = \mathbf{k} * \mathbf{C} \quad (4)$$

Initially the activity of photocatalyst is 1, as we use fresh photocatalyst. The catalyst activity, **a**, was defined as:

$$\mathbf{a} = \mathbf{r_{0i}} / \mathbf{r_0} \quad (5)$$

where $\mathbf{r_{0i}}$ is the initial rate of reaction for ith cycle and $\mathbf{r_0}$ is de initial rate of reaction for 1st cycle. The loss of activity was examined based on repeatedly the same sample under MB degradation and irradiation for four successive cycles. The loss of activity was calculated from:

$$\mathbf{a = a_0 * e^{-k_d * t}} \quad (6)$$

where $\mathbf{a}$ is the activity of photocatalyst, $\mathbf{k_d}$ is the photocatalyst deactivation constant. Fitting the value of catalyst activity against starting time of each cycle from table 1 we get the next equations:

$$\mathbf{a_{T10} = 1.05 * e^{-0.0903*t}} \quad (7) \qquad \mathbf{a_{T11} = 1.00 * e^{-0.0818*t}} \quad (8)$$

The activity of photocatalyst at any time can be calculated from equations 8 and 9. The values of photocatalyst deactivation constant are 0.0903 h^{-1} and 0.0818 h^{-1} for the samples T10 and T11, respectively.

After an ultrasonic treatment in tri-distillated water for 10 minutes, the degradation rate of MB solution, the kinetics constants and catalyst activities were recovered around to their initial values. It is due to the intermediate products are removed from the active sites of TiO_2 thin film surface. These results show that recycling of thin film is also possible with it regeneration. These characteristics make them suitable for technological applications, such as organic degradation in effluent cleaning systems. Figure 10 shows the MB concentration ratio vs time plot for successive cycles. The starting time of each cycle was cumulative, because the activity of the TiO_2 thin film decreases due to poising. Additionally, the activity of the samples decreases after each cycle due to effect of intermediate product and some inorganic ions [27]. These intermediate products interfere to the process left inactive sites on TiO_2 thin film surface.

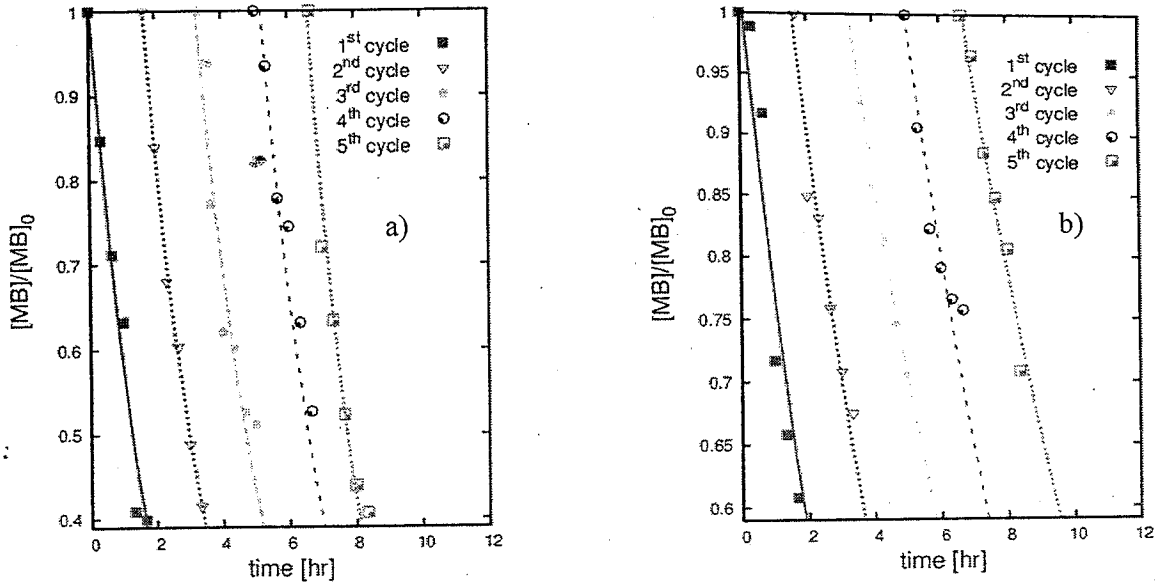

Figure 10. MB concentration ratio vs. time plot for successive cycles for a) TiO_2 thin film deposited at 1 step and b) TiO_2 thin film deposited at 2 steps. The points denote experimental data and lines indicate model equations.

References

[1] A. Fujishima, K. Honda, Electrochemical photolysis of water at a semiconductor electrode, Nature 238 (1972) 37-38.

[2] M.P. Seabra, R.R. Pires, J.A. Labrincha, Ceramic tiles for photodegradation of Orange II solutions, Chemical Engineering Journal 171 (2011) 692-702.

[3] W. Jun, Z. Gang, Z. Zhaohong, Z. Xiangdong, Z. Guan, M. Teng, J. Yuefeng, Z. Peng, L. Ying, Investigation on degradation of azo fuchsine using visible light in the presence of heat-treated anatase TiO_2 powder, Dyes and Pigments 75 (2007) 335-343.

[4] P. Amézaga-Madrid, R. Silveyra-Morales, L. Córdoba-Fierro, G.V. Nevárez-Moorillón, M. Miki-Yoshida, E. Orrantia-Borunda, F.J. Solís, TEM evidence of ultrastructural alteration on *Pseudomonas aeruginosa* by photocatalytic TiO_2 thin films, Journal of Photochemistry and Photobiology B: Biology 70 (2003) 45-50.

[5] Z. Nagamedianova, R.E. Ramírez-García, S.V. Flores-Arévalo, M. Miki-Yoshida, M. Arroyo-Ortega, Solar heat reflective glass by nanostructured sol–gel multilayer coatings, Optical Materials 33 (2011) 1999–2005.

[6] K. Hashimoto, H. Irie, A. Fujishima, TiO_2 photocatalysis: a historical overview and future prospects, Jpn. J. Appl. Phys. 44 (2005) 8269-8285.

[7] J. Du, W. Chen, C. Zhang, Y. Liu, C. Zhao, Y. Dai, Hydrothermal synthesis of porous TiO_2 microspheres and their photocatalytic degradation of gaseous benzene, Chemical Engineering Journal, 170 (2011) 53-58. (2003) 45–50.

[8] W.S. Kuo, P.H. Ho, Solar photocatalytic decolorization of dyes in solution with TiO_2 film, Dyes and Pigments 71 (2006) 212-217.

[9] L.M. Saragiotto, H.J. Alves, O.A. Andreo, C.M. Macedo, Discoloration and degradation of textile dye aqueous solutions with titanium oxide catalysts obtained by the sol-gel method, Dyes and Pigments 76 (2008) 525-529.

[10] M. Toyoda, Y. Nanbu, Y. Nakazawa, M. Hirano, M. Inagaki, Effect of crystallinity of anatase on photoactivity for methylene blue decomposition in water, Applied Catalysis B: Enviromental 49 (2004) 227-232.

[11] D. Wang, X. Li, J. Chen, X. Tao, Enhanced photoelectrocatalytic activity of reduced graphene oxide/TiO_2 composite films for dye degradation, Chemical Engineering Journal, article in press (2012).

[12] Y. Kikuchi, K. Sunada, T. Iyoda, K. Hashimoto, A. Fujishima, Photocatalytic bactericidal effect of TiO_2 thin films: dynamic view of the active oxygen species responsible for the effect, Journal of Photochemistry and Photobiology A: Chemistry 106 (1997) 51-56.

[13] M. Miki-Yoshida, W. Antúnez-Flores, K. Gomez-Fierro, L. Villa-Pando, R. Silveyra-Morales, P. Sánchez-Santiago, R. Martínez-Sánchez, M. José-Yacamán, Growth and structure of TiO_2 thin films deposited inside borosilicate tubes by spray pyrolysis, Surface & Coatings Technology 200 (2006) 4111 – 4116.

[14] Y. Chen, D.D. Dionysiou, TiO_2 photocatalytic films on stainless steel: the role of Degussa P-25 in modified sol-gel methods, Appl. Catal. B-Environ. 62 (2006) 255-264.

[15] F. Meng, X. Song, Z. Sun, Photocatalytic activity of TiO_2 thin films deposited by Rf magnetron sputtering, Vacuum 83 (2009) 1147-1151.

[16] M.F. Brunilla, M.V. Diamanti, M.P. Pedeferri, F. Di Fonzo, C.S. Casari, A. Li Bassi, Photocatalytic behavior of different titanium dioxide layers, Thin Solid Films 515 (2007) 6309-6313.

[17] P. Amézaga-Madrid, W. Antúnez-Flores, J.E. Ledezma-Sillas, J.G. Murillo-Ramírez, O. Solís-Canto, O.E. Vega-Becerra, R. Martínez-Sánchez, M. Miki-Yoshida, Synthesis, microstructural characterization and optical properties of undoped, V and Sc doped ZnO thin films, Journal of Alloys and Compounds (2011), Article in press.

[18] E. Ríos-Valdovinos, P. Amézaga-Madrid, J. Pola-Albores, P. Pizá-Ruiz, M. Miki-Yoshida. Sistema para depositar películas delgadas de metales, materiales semiconductores, materiales dieléctricos o polímeros en la superficie interior o exterior de un tubo usando la técnica de depósito químico de vapor asistido por aerosol. Mexican Patent Application MX/a/2012/005462.

[19] B.D. Cullity, Elements of X-Ray Difracction, Addison-Wesley Metallurgy Series (1956) 99.

[20] Joint Committee on Powder Diffraction Standards, Powder Diffraction File, International Center for Diffraction Data, Newtown Square, Swarthmore, PA, 2011.

[21] M.L. Hitchman, J. Zhao, The LPCVD of rutile at low temperatures, J. Physique IV 9 (1999) 348.

[22] K.H. Wang, Y.H. Hsieh, T.T. Lin, C.Y. Chang, Effects of temperature on the properties of TiO_2 photocatalysts prepared by the chemical vapor deposition (CVD) method, React. Kinets Catal. Lett., Vol. 95, 1 (2008) 39-46.

[23] T. Ohsaka, F. Izumi, Y. Fujiki, Raman spectrum of anatase, TiO_2, Journal of Raman spectroscopy 7 (1978) 321–324.

[24] M.A. Rauf, S.S. Ashraf, Fundamental principles and application of heterogeneous photocatalytic degradation of dyes in solution, Chemical Engineering Journal 151 (2009) 10-18.

[25] A. Houas, H. Lachheb, M. Ksibi, E. Elaloui, C. Guillard, J. M. Hermann, Photocatalytic degradation pathway of methylene blue in water, App Catal B- Environ 31 (2001) 145-157.

[26] C.M. Malengreaux, A. Timmermans, S.L. Pirard, S.D. Lambert, J-P. Pirard, D. Poelman, B. Heinrichs, Optimized deposition of TiO_2 thin films produced by a non-aqueous sol-gel method and quantification of their photocatalytic activity, Chemical Engineering Journal, article in press (2012).

[27] H. Lachheb, E. Puzenat, A. Houas, M. Ksibi, E. Elaloui, C. Guillard, J-M. Herrmann, Photocatalytic degradation of various types of dyes (Alizarin S, Crocein Ornage G, Methyl Red, Congo Red, Methylene Blue) in water by UV-irradiated titania.